Inorganic Chemistry

Article

pubs.acs.org/IC

Efficient Sensitization of Dye-Sensitized Solar Cells by Novel Triazine-Bridged Porphyrin−Porphyrin Dyads

Galateia E. Zervaki,[†] Mahesh S. Roy,[‡] Manas K. Panda,[†] Panagiotis A. Angaridis,[†] Emmanouel Chrissos,[†] Ganesh D. Sharma,*[,§] and Athanassios G. Coutsolelos*[,†]

[†]Laboratory of Bioinorganic Chemistry, Department of Chemistry, University of Crete, Voutes Campus, P.O. Box 2208, 71003 Heraklion, Crete, Greece

[§]R&D Center for Engineering and Science, JEC Group of Colleges, Jaipur Engineering College, Kukas, Jaipur (Raj.) 303101, India

[‡]Defence Laboratory, Jodhpur (Raj.) 342011, India

Supporting Information

ABSTRACT: Two novel porphyrin−porphyrin dyads, the symmetrical Zn[Porph]−Zn[Porph] (**2**) and unsymmetrical Zn[Porph]−H_2[Porph] (**4**), where Zn[Porph] and H_2[Porph] are the metalated and free-base forms of 5-(4-aminophenyl)-10,15,20-triphenylporphyrin, respectively, in which two porphyrin units are covalently bridged by 1,3,5-triazine, have been synthesized via the stepwise amination of cyanuric chloride. The dyads are also functionalized by a terminal carboxylic acid group of a glycine moiety attached to the triazine group. Photophysical measurements of **2** and **4** showed broaden and strengthened absorptions in their visible spectra, while electrochemistry experiments and density functional theory calculations revealed negligible interaction between the two porphyrin units in their ground states but appropriate frontier orbital energy levels for use in dye-sensitized solar cells (DSSCs). The **2**- and **4**-based solar cells have been fabricated and found to exhibit power conversion efficiencies (PCEs) of 3.61% and 4.46%, respectively (under an illumination intensity of 100 mW/cm^2 with TiO_2 films of 10 μm thickness). The higher PCE value of the **4**-based DSSC, as revealed by photovoltaic measurements ($J-V$ curves) and incident photon-to-current conversion efficiency (IPCE) spectra of the two cells, is attributed to its enhanced short-circuit current (J_{sc}) under illumination, high open-circuit voltage (V_{oc}), and fill factor (FF) values. Electrochemical impedance spectra demonstrated shorter electron-transport time (τ_d), longer electron lifetime (τ_e), and high charge recombination resistance for the **4**-based cell, as well as larger dye loading onto TiO_2.

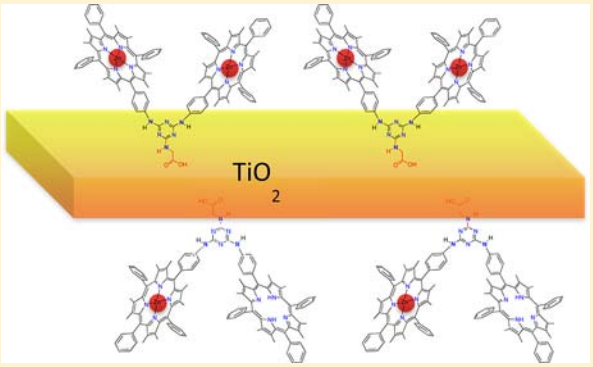

INTRODUCTION

Dye-sensitized solar cells (DSSCs) are currently attracting considerable attention as alternatives to conventional amorphous silicon-based solar cells because of their low production cost, simplicity of fabrication, and high power conversion efficiency (PCE). In these devices, a thin layer of a sensitizer (a chromophore), chemically bound to nanoporous TiO_2, is photoexcited and ultimately provides the photocurrent.[1] Among the most efficient DSSC sensitizers are ruthenium polypyridyl complexes, which exhibit intense and wide-range absorption from the visible to near-IR regime[2] and attain cell efficiencies above 11%.[3] However, because of their high cost and environmental concerns, their wide application is limited. Metal-free organic dyes have also been used as sensitizers,[4] but the most efficient ones result in cell efficiencies in the range of 9−10%.[5] A lot of effort is currently devoted to the development of new, efficient chromophores that exhibit strong and panchromatic absorption and good light-harvesting efficiency and are suitable for practical use.[6]

Porphyrins, owing to their light-harvesting potential (exemplified by their role in photosynthesis) and their physicochemical properties, is a class of compounds that stimulated significant research interest as artificial antennae in solar cells.[7] Porphyrin derivatives exhibit intense absorption in the visible regime (a strong Soret band in the 450−500 nm region and moderate Q bands in the 550−650 nm region).[8] In addition, their frontier orbital energy levels allow for efficient electron injection into the TiO_2 band and regeneration of the oxidized dye by the electrolyte in a solar cell. Furthermore, by appropriate functionalization of the porphyrin ring, either in the meso or β positions, their spectral and redox properties can be tuned, allowing control of the solar cell efficiency. Over the last years, a large number of reports on porphyrin-based solar cells with remarkable performances appeared in the literature.[9] Campbell et al. were the first to report in 2007 a DSSC based on a porphyrin with a conjugated, dicarboxylic acid anchoring

Received: March 28, 2013
Published: August 14, 2013

   dx.doi.org/10.1021/ic400774p | *Inorg. Chem.* 2013, 52, 9813−9825

Scheme 1

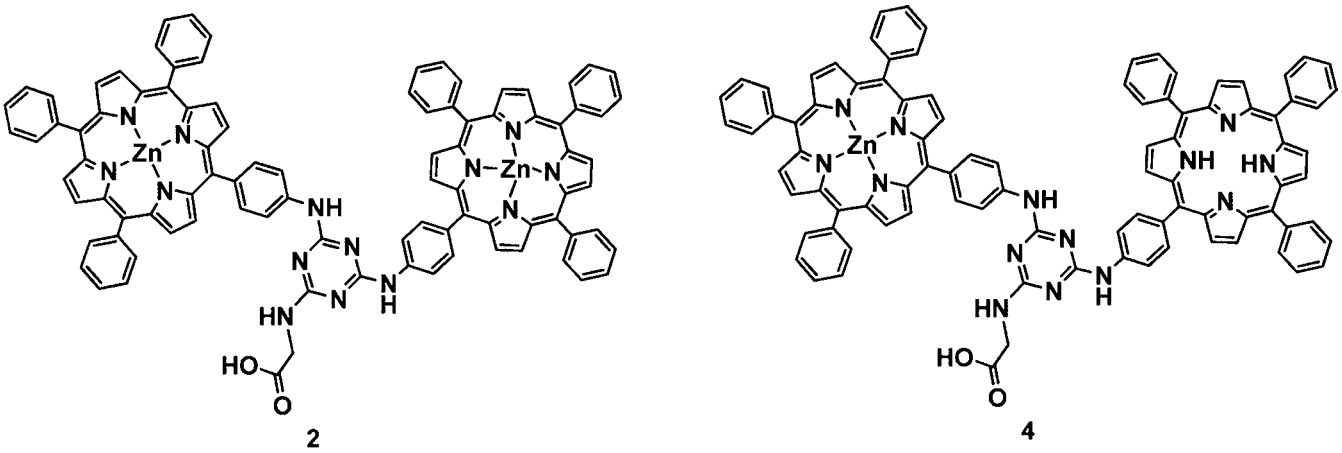

group that gave a cell PCE above 7%.[10] In 2010, Bessho et al., by introducing donor−acceptor (or "push−pull") porphyrins, raised the cell efficiencies to 11%.[11] In 2011, Grätzel and coworkers synthesized a "push−pull" zinc-metalated porphyrin that, in combination with an organic cosensitizer and a cobalt-based electrolyte, achieved the remarkable cell efficiency of 12.3%, the highest cell efficiency hitherto reported for DSSCs.[12] Additionally, Wang et al. reported a porphyrin-based DSSC that, without cosensitization, gave a cell PCE above 10%.[13]

One of the intrinsic limitations of porphyrins is their relatively narrow absorbing range and weak light-harvesting ability in the green and red regions of the solar spectrum, affecting their overall performance in DSSCs. Nevertheless, by incorporating covalently linked arrays of porphyrin units absorbing in different spectral regions, panchromatic sensitization and enhancement of the overall light-harvesting capacity might be achieved. Indeed, examples from the literature reveal that multiporphyrin arrays lead to DSSCs with increased light-harvesting ability, but the cell efficiencies depend on the type of linkage between the porphyrin units. For example, porphyrin dyads (the simplest multiporphyrin arrays), with the porphyrin units linked through their peripheral aryl groups by an ether bridge, resulted in cells with low efficiency because of very poor communication between the porphyrin units.[14] However, when the two porphyrin units are linked through their meso positions, either directly[15] or by a suitable π-conjugated linker,[16] broadening of spectral coverage and improved light-harvesting properties have been observed. Furthermore, it has been proposed that unsymmetrical porphyrin dyads can lead to enhancement of the overall solar cell efficiency.[17]

In present work, we report the synthesis of two novel porphyrin−porphyrin dyads, the symmetrical Zn[Porph]−Zn[Porph] (**2**) and unsymmetrical Zn[Porph]−H_2[Porph] (**4**), where Zn[Porph] and H_2[Porph] are the metalated and free-base forms of 5-(4-aminophenyl)-10,15,20-triphenylporphyrin, respectively. The porphyrin units are covalently linked through peripheral arylamino groups by 1,3,5-triazine, which is further functionalized by a terminal carboxylic acid group (Scheme 1). 1,3,5-Triazine is a known mediator of intramolecular photoinduced electron transfer between two or three chromophores. Furthermore, the broaden and strengthened spectral absorptions of **2** and **4**, together with their appropriate frontier orbital energy levels, make them promising candidates as efficient sensitizers in DSSCs. The PCEs of the **2**- and **4**-based solar cells were found to be 3.61% and 4.46%, respectively. Photovoltaic measurements as well as incident photon-to-current conversion efficiency (IPCE) and electrochemical impedance spectroscopy (EIS) spectra of the two cells revealed enhanced short-circuit current (J_{sc}) under illumination, higher open-circuit voltage (V_{oc}), and fill factor (FF) values for the DSSC sensitized by the unsymmetrical dyad **4**, which are related to its shorter electron-transport time (τ_d), longer electron lifetime (τ_e), and larger dye loading onto the TiO_2 surface.

EXPERIMENTAL SECTION

Materials and Techniques. All manipulations were carried out using standard Schlenk techniques under a nitrogen atmosphere. 2,4,6-Trichloro-1,3,5-triazine (cyanuric chloride), diisopropylethylamine (DIPEA), glycine methyl ester hydrochloride, $Zn(CH_3COO)_2{\cdot}2H_2O$, Na_2SO_4, KOH, and other chemicals and solvents were purchased from the usual commercial sources and used as received, unless otherwise stated. Tetrahydrofuran (THF) was freshly distilled from sodium/benzophenone. 5-(4-Aminophenyl)-10,15,20-triphenylporphyrin (H_2[TPP-NH_2]) and 5-(4-aminophenyl)-10,15,20-triphenylporphyrinatozinc (Zn[TPP-NH_2]) were prepared according to literature procedures.[18]

Synthesis of 5-[4-[3-[5-(4-Aminophenyl)-10,15,20-triphenylporphyrinato]-5-(glycine methyl ester)triazinyl]aminophenyl]-10,15,20-triphenylporphyrin (1). To a THF solution (1 mL) of cyanuric chloride (14.6 mg, 0.079 mmol) and DIPEA (17 μL, 0.095 mmol) was added a THF solution (1 mL) of H_2[TPP-NH_2] (50 mg, 0.079 mmol) under argon at 0 °C. The mixture was stirred at 0 °C for 15 min, and upon reaction completion [monitored by thin-layer chromatography (TLC)], it was left to warm at room temperature. Next, a THF solution (4 mL) of H_2[TPP-NH_2] (100 mg, 0.16 mmol) and DIPEA (33 μL, 0.19 mmol) was added, and the mixture was stirred at room temperature overnight. An excess of glycine methyl ester hydrochloride (100 mg, 0.79 mmol) and DIPEA (0.3 mL, 1.9 mmol) were added, and the mixture was stirred at 65 °C for 24 h. The volatiles were removed under reduced pressure, and after dilution in CH_2Cl_2, the residue was purified by column chromatography (silica gel, CH_2Cl_2/EtOH 5%). The product **1** was isolated as a purple solid. Yield: 40 mg (36%). ^{1}H NMR (300 MHz, $CDCl_3$): δ 8.97 (s, 4H), 8.84 (s, 12H), 8.18 (m, 17H), 7.72 (m, 18H), 7.55 (s, 4H), 6.06 (s, 2H), 4.40 (d, J = 5.4 Hz, 2H), 3.82 (s, 3H), −2.75 (s, 4H). HRMS (MALDI-TOF). Calcd for $C_{94}H_{67}N_{14}O_2$: m/z 1424.5493 ([M + H]$^+$). Found: m/z 1424.5504. UV−vis [CH_2Cl_2; λ, nm (ε, $\times10^{-3}$ M^{-1} cm^{-1})]: 419 (540.4), 516 (26.3), 552 (11.2), 590 (8.5), 647 (6.4). Anal. Calcd for $C_{94}H_{66}N_{14}O_2$: C, 79.31; H, 4.67; N, 13.77. Found: C, 79.22; H, 4.75; N, 13.65.

Synthesis of 5-[4-[3-[5-(4-Aminophenyl)-10,15,20-triphenylporphyrinato]zinc-5-glycinetriazinyl]aminophenyl]-10,15,20-triphenylporphyrin Zinc (2). *Metalation.* To a CH_2Cl_2

dx.doi.org/10.1021/ic400774p | Inorg. Chem. 2013, 52, 9813−9825

solution (12 mL) of **1** (40 mg, 0.028 mmol) was added a saturated MeOH solution (4 mL) of $Zn(CH_3COO)_2{\cdot}2H_2O$ in MeOH (500 mg/20 mL), and the reaction mixture was stirred at room temperature overnight. The organic phase was washed with H_2O (3 × 10 mL) and dried with Na_2SO_4, and the solvent was removed under reduced pressure. The crude product **1-Zn$_2$** was purified by column chromatography (silica gel, CH_2Cl_2/EtOH 1%), resulting in 36 mg of a purple solid (yield: 90%). ^{1}H NMR (300 MHz, $CDCl_3$): δ 9.04 (s, 5H), 8.93 (s, 11H), 8.17 (m, 16H), 7.88 (m, 5H), 7.70 (m, 17H), 7.02 (s, 1H), 4.01 (d, J = 5.4 Hz, 2H), 3.61 (s, 3H). The absence of the hydrogen signals due to the amide groups has very low intensity, and they are probably masked under stronger signals in the aromatic region. HRMS (MALDI-TOF). Calcd for $C_{94}H_{63}N_{14}O_2Zn_2$: m/z 1547.3763 ($[M + H]^+$). Found: m/z 1547.3742. UV−vis [CH_2Cl_2; λ, nm (ε, $\times 10^{-3}$ M^{-1} cm^{-1})]: 422 (783.2), 550 (33.8), 591 (10.5). Anal. Calcd for $C_{94}H_{62}N_{14}O_2Zn_2$: C, 72.82; H, 4.03; N, 12.65. Found: C, 72.77; H, 4.14; N, 12.61.

Ester Hydrolysis. To a THF solution (15 mL) of the product isolated from the metalation reaction (36 mg, 0.023 mmol) were added 4.8 mL of MeOH, 6 mL of H_2O, and KOH (450 mg, 0.008 mol). The reaction mixture was stirred at room temperature overnight. The organic solvents were removed under reduced pressure, and then a solution of HCl (1.5 M) was added dropwise, until pH ∼5. The precipitate was filtered, washed with H_2O, extracted with CH_2Cl_2, and purified by column chromatography (silica gel, CH_2Cl_2/EtOH 5%). The product **2** was isolated as a purple solid. Yield: 30 mg (85%). ^{1}H NMR (300 MHz, $CDCl_3$, MeOD): δ 8.86 (s, 5H), 8.74 (s, 11H), 8.05 (m, 17H), 7.57 (m, 22H), 6.50 (s, 2H), 4.08 (s, 2H). The absence of any signal due to the amide groups as well as the pyrrolic hydrogen atoms of the free-base porphyrin is attributed to H/D exchange caused by MeOD. ^{13}C NMR (75 MHz, $CDCl_3$, MeOD): δ 150.2, 149.9, 144.0, 143.3, 138.0, 134.9, 134.4, 131.5, 127.1, 126.2, 120.5, 120.3, 118.4, 29.7, 29.3. HRMS (MALDI-TOF). Calcd for $C_{93}H_{62}N_{14}O_2Zn_2$: m/z 1534.3607 ($[M + 2H]^+$). Found: m/z 1534.3576. UV−vis [CH_2Cl_2; λ, nm (ε, $\times 10^{-3}$ M^{-1} cm^{-1})]: 425 (627.9), 556 (29.5), 596 (12.0). Anal. Calcd for $C_{93}H_{60}N_{14}O_2Zn_2$: C, 72.71; H, 3.94; N, 12.76. Found: C, 72.79; H, 4.02; N, 12.68.

Synthesis of 5-[4-[3-[5-(4-Aminophenyl)-10,15,20-triphenylporphyrinato]-5-(glycine methyl ester)triazinyl]aminophenyl)-10,15,20-triphenylporphyrin Zinc (3). A THF solution (1 mL) of Zn[TPP-NH_2] (50 mg, 0.072 mmol) was added to a THF solution (1 mL) of cyanuric chloride (13.3 mg, 0.072 mmol) and DIPEA (15 μL, 0.086 mmol) under argon at 0 °C. The mixture was stirred at 0 °C for 15 min, and upon reaction completion (monitored by TLC), it was left to warm at room temperature. Then, a THF solution (4 mL) of H_2[TPP-NH_2] (90.7 mg, 0.144 mmol) and DIPEA (30 μL, 0.173 mmol) was added, and the mixture was stirred at room temperature overnight. Glycine methyl ester hydrochloride (90.4 mg, 0.72 mmol) and DIPEA (0.3 mL, 1.9 mmol) were added, and the mixture was stirred at 65 °C for 24 h. The volatiles were removed under reduced pressure, and after dilution in CH_2Cl_2, the residue was purified by column chromatography (silica gel, CH_2Cl_2/EtOH 5%). The product **3** was isolated as a purple solid. Yield: 38 mg (34%). ^{1}H NMR (300 MHz, $CDCl_3$): δ 9.05 (d, J = 4.5 Hz, 2H), 8.93 (s, 7H), 8.82 (s, 7H), 8.20 (m, 15H), 8.02 (d, J = 8.1 Hz, 4H), 7.71 (m, 19H), 5.68 (s, 2H), 4.28 (d, J = 5.1 Hz, 2H), 3.77 (s, 3H), −2.75 (s, 2H). The absence of the hydrogen signals due to the amide group has very low intensity, and they are probably masked under stronger signals in the aromatic region. HRMS (MALDI-TOF). Calcd for $C_{94}H_{65}N_{14}O_2Zn$: m/z 1485.4628 ($[M + H]^+$). Found: m/z 1485.4642. UV−vis [CH_2Cl_2; λ, nm (ε, $\times 10^{-3}$ M^{-1} cm^{-1})]: 421 (696.0), 515 (21.3), 551 (25.0), 591 (10.6), 646 (5.3). Anal. Calcd for $C_{94}H_{64}N_{14}O_2Zn$: C, 75.93; H, 4.34; N, 13.19. Found: C, 75.82; H, 4.43; N, 13.27.

Synthesis of 5-[4-[3-[5-(4-Aminophenyl)-10,15,20-triphenylporphyrinato]-5-glycinetriazinyl]aminophenyl]-10,15,20-triphenylporphyrin Zinc (4). To a THF solution (15 mL) of **3** (30 mg, 0.020 mmol) were added 4.8 mL of MeOH, 6 mL of H_2O, and KOH (450 mg, 0.008 mol). The reaction mixture was stirred at room temperature overnight. The organic solvents were removed under reduced pressure, and then a solution of HCl (1.5 M) was added dropwise, until pH ∼5. The precipitate was filtered, washed with water, extracted with CH_2Cl_2, and purified by column chromatography (silica gel, CH_2Cl_2/EtOH 10%). The product **4** was isolated as a purple solid. Yield: 25 mg (85%). ^{1}H NMR (300 MHz, $CDCl_3$/MeOD = 1/0.01): δ 8.76 (m, 16H), 7.90 (m, 28H), 6.56 (s, 2H), 4.15 (s, 2H). The absence of any signal due to the amide groups as well as the pyrrolic hydrogen atoms of the free-base porphyrin is attributed to H/D exchange caused by MeOD. HRMS (MALDI-TOF). Calcd for $C_{93}H_{63}N_{14}O_2Zn$: m/z 1471.4472 ($[M + H]^+$). Found: m/z 1471.4505. UV−vis [toluene; λ, nm (ε, $\times 10^{-3}$ M^{-1} cm^{-1})]: 422 (442.5), 517 (17.9), 552 (20.7), 592 (8.6), 648 (4.6). Anal. Calcd for $C_{93}H_{62}N_{14}O_2Zn$: C, 75.83; H, 4.24; N, 13.31. Found: C, 75.77; H, 4.16; N, 13.42.

NMR Spectra. ^{1}H and ^{13}C NMR spectra were recorded on a Bruker DPX-300 MHz spectrometer as solutions in deuterated solvents using the solvent peak as the internal standard.

Mass Spectra. High-resolution mass spectrometry (HRMS) spectra were recorded on a Bruker UltrafleXtreme MALDI-TOF/TOF spectrometer.

FTIR Spectra. FTIR were recorded on a Perkin-Elmer 16PC FTIR spectrometer.

Photophysical Measurements. UV−vis absorption spectra were measured on a Shimadzu UV-1700 spectrophotometer using 10-mm-path-length cuvettes. Emission spectra were measured on a JASCO FP-6500 fluorescence spectrophotometer equipped with a red-sensitive WRE-343 photomultiplier tube (wavelength range 200−850 nm). Emission lifetimes were determined by the time-correlated single-photon-counting technique using an Edinburgh Instruments mini-τ lifetime spectrophotometer equipped with an EPL 405 pulsed diode laser at 406.0 nm with a pulse width of 71.52 ps and pulse periods of 200 and 100 ns and a high-speed red-sensitive photomultiplier tube (H5773-04) as the detector.

Electrochemistry. Cyclic and square-wave voltammetry experiments were carried out at room temperature using an AutoLab PGSTAT20 potentiostat and appropriate routines available in the operating software (*GPES*, version 4.9). Measurements were carried out for **2** and **4** in freshly distilled and deoxygenated THF, with a scan rate of 20 mV/s, and for **1-Zn$_2$** and **3** in freshly distilled and deoxygenated CH_2Cl_2, using a scan rate of 100 mV/s, with a solute concentration of 1.0 mM in the presence of tetrabutylammonium hexafluorophosphate (0.1 M) as the supporting electrolyte. A three-electrode cell setup was used with platinum as the working electrode, a saturated calomel (SCE) reference electrode, and a platinum wire as the counter electrode.

Computational Methods. Density functional theory (DFT) calculations[19] were performed using the *Gaussian 03* program suite.[20] Gas-phase geometry optimizations were carried out by employing Becke three-parameter exchange in conjunction with the Lee−Yang−Parr correlation functional (B3LYP).[21,22] For geometry optimizations, the LANL2DZ basis set was used for zinc atoms and the 6-31G(d) basis set for lighter atoms. The input geometries were modeled using *ChemCraft* software.[23] The optimized minimum-energy structures were verified as stationary points on the potential energy surface by vibrational frequency analysis calculation. Time-dependent DFT (TDDFT) calculations were performed using the gas-phase-optimized structures in CH_2Cl_2 with standard dielectric constant ε = 8.93. Solvent effects were evaluated using the polarizable continuum model implemented in *Gaussian 03*, in which the cavity is generated via overlapping spheres, previously developed by Tomasi et al.[24,25] For the TDDFT calculations, the LANL2DZ basis set was used for zinc atoms and the 6-311G* basis set for lighter atoms. A total of 20 lowest-energy, spin-allowed, singlet transitions were used to simulate the absorption spectra. Computed structures and molecular orbitals were visualized and analyzed by *ChemCraft* software.

Cell Fabrication. The DSSCs were fabricated with electrodes based on fluorine-doped tin oxide (FTO)-coated glass substrates, which were precleaned with deionized water, acetone, and ethanol and then dried in air. For the working electrode, TiO_2 paste, prepared as reported earlier,[26] was deposited on the FTO substrate by the doctor blade technique. TiO_2 films of different thicknesses were prepared (4, 6, 8, 10, and 12 μm) in order to optimize the photovoltaic

dx.doi.org/10.1021/ic400774p | *Inorg. Chem.* 2013, 52, 9813−9825

Scheme 2

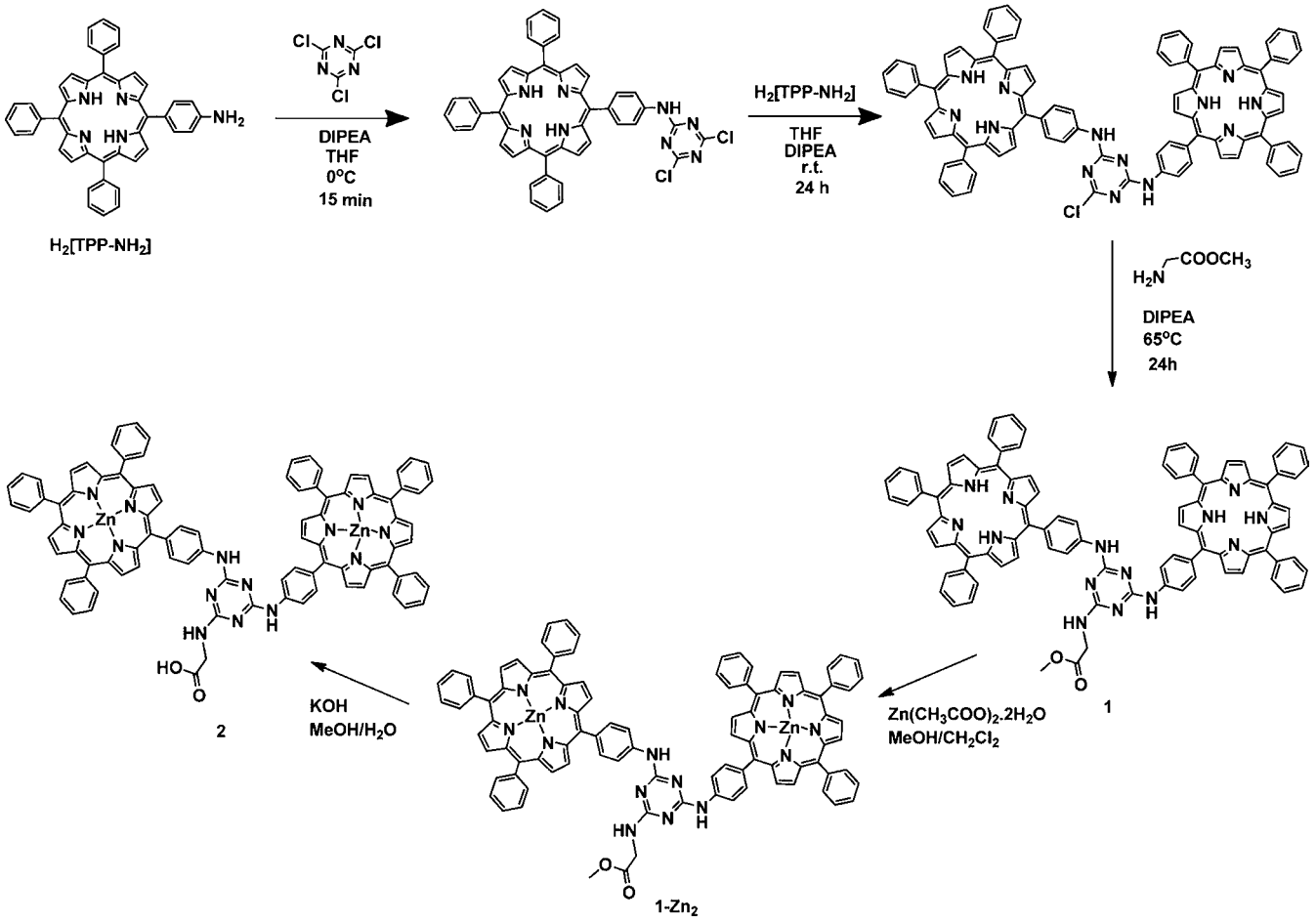

Scheme 3

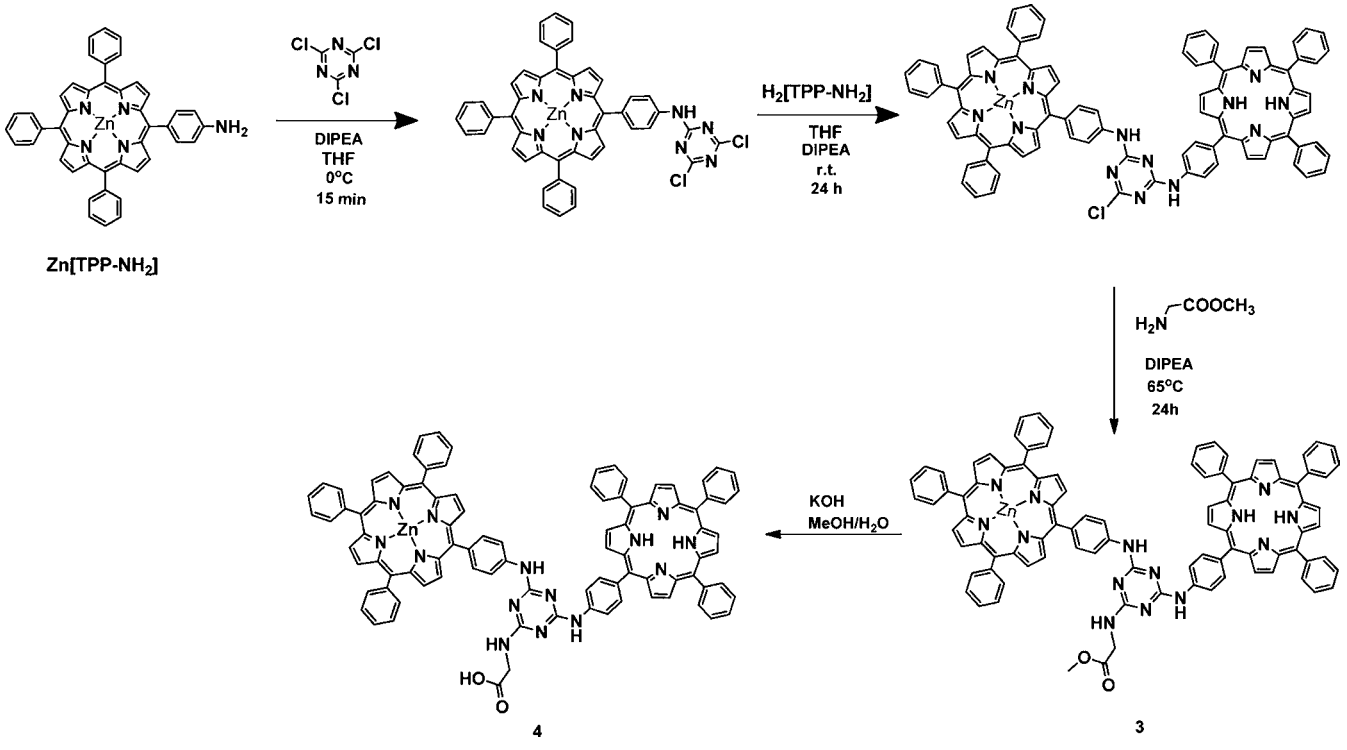

dx.doi.org/10.1021/ic400774p | Inorg. Chem. 2013, 52, 9813−9825

performance of DSSCs. In all cases, the electrode was sintered at 450 °C for 30 min. After cooling to room temperature, it was immersed in a 20 mM $TiCl_4$ aqueous solution for 30 min at 80 °C, washed with deionized water and ethanol, sintered again at 450 °C for 30 min, and cooled at 60 °C. Finally, it was immersed in a porphyrin solution (200 μM in $CHCl_3$/EtOH = 1/1, containing 20 mM chenodeoxycholic acid as an aggregation inhibitor) for 12 h to give the porphyrin-sensitized TiO_2 working electrode. The platinum wire counter electrode was prepared by spin-coating drops of a H_2PtCl_6 solution onto a FTO-coated glass substrate and heating at 350 °C for 15 min. The DSSCs were assembled by separating the working electrode from the counter electrode by a 20-μm-thick Surlyn hot-melt gasket. In the space between the working and counter electrodes, the electrolyte [consisting of 0.05 M I_2, 0.5 M LiI, 0.6 M (dimethylpropyl)-benzimidiazole iodide, 0.5 M 4-*tert*-butylpyridine in an acetonitrile solution] was introduced through a hole and sealed with Surlyn.

The current−voltage (J−V) characteristics of the DSSCs under illumination were measured by a Keithley sourcemeter and a solar simulator coupled with a 150 W xenon lamp and an AM optical filter to give 100 mW/cm^2 illumination at the DSSC surface. The EIS spectra, in the dark and under illumination, were recorded using an electrochemical workstation (Autolab PGSTAT) with s frequency response analyzer. The frequency range was from 10 mHz to 100 kHz, and an alternating-current potential of 10 mV was used. A direct-current bias equivalent to the open-circuit voltage of DSSC was applied. The impedance data were analyzed using *Z-View* software with an appropriate equivalent circuit. The IPCE was measured as a function of the wavelength with a xenon lamp, a monochromator, and a Keithley sourcemeter at 1 mW/cm^2. The intensity calibration for the IPCE measurement was performed using a standard silicon photodiode.

RESULTS AND DISCUSSION

Synthesis and Characterization. The syntheses of the symmetrical dyad Zn[Porph]−Zn[Porph] (**2**) and unsymmetrical dyad Zn[Porph]−H_2[Porph] (**4**) are presented in Schemes 2 and 3, respectively. In both dyads, the porphyrin units are covalently linked through their peripheral arylamino groups by a 1,3,5-triazine group. The third position of the triazine group is functionalized by a carboxylic acid of a glycine moiety (as an anchoring group for attachment on the TiO_2 surface of DSSC electrodes).

The precursor of 1,3,5-triazine, cyanuric chloride, is a commercially available and inexpensive reagent that has been extensively used in a variety of chemical transformations[27] and as a template for the synthesis of macrocycles,[28] dendrimers,[29] and multiporphyrin arrays.[30,31] Its reactivity is based on the temperature-dependent stepwise substitution of its three chlorine atoms and the sequential introduction of different nucleophiles. As a result, it allows the use of one-pot protocol reactions, providing a modular synthetic route to the desired multiporphyrin arrays in good yields and avoiding extensive and expensive preparative and purification procedures. Furthermore, it offers a simple route to the challenging synthesis of unsymmetrical multiporphyrin arrays bearing different chromophores (in our case, zinc-metalated and free-base porphyrins), which are difficult to synthesize with respect to symmetrical dyads.

Symmetrical dyad **2** was prepared in a one-pot reaction, starting from cyanuric chloride and H_2[TPP-NH_2] in the presence of the base DIPEA at 0 °C in THF. Monitoring of the reaction by TLC indicated the disappearance of the reactants and the formation of the free-base monoporphyrin triazine. The latter was neither isolated nor characterized and further reacted at room temperature with 1 equiv of H_2[TPP-NH_2], resulting in the symmetrical free-base porphyrin dyad. Substitution of the third chlorine atom of cyanuric chloride by a glycine methyl ester moiety took place at 65 °C in the same pot and gave the symmetrical, free-base porphyrin dyad **1**, as confirmed by ^{1}H NMR spectroscopy and MALDI-TOF spectrometry. It should be noted that, in the ^{1}H NMR spectrum of **1**, the signals for the aromatic hydrogen atoms ortho to the H_2[TPP-NH_2] amino groups were downfield displaced after attachment to the triazine ring. Its UV−vis absorption spectrum in CH_2Cl_2, except from the Soret band at 419 nm, exhibits four Q bands at 516, 552, 590, and 647 nm, which is characteristic of free-base porphyrins.

The reaction of **1** with an excess of $Zn(CH_3COO)_2{\cdot}2H_2O$ in MeOH/CH_2Cl_2 gave **1-Zn$_2$**, while basic hydrolysis of the methyl ester group of **1-Zn$_2$**, followed by aqueous workup and chromatographic separation, resulted in almost quantitative conversion to the symmetrical zinc-metalated dyad **2**, as confirmed by ^{1}H and ^{13}C NMR and UV−vis absorption spectroscopy and MALDI-TOF spectrometry. The most noticeable feature in the ^{1}H NMR spectrum of **2**, with respect to the analogous free-base dyad **1**, is the disappearance of the pyrrolic hydrogen atom's signal at −2.75 ppm. Also, after ester hydrolysis, the absence of the signal at 3.82 ppm of the methyl ester protons is obvious. The UV−vis absorption spectrum of **2** in CH_2Cl_2 shows only two Q bands at 556 and 596 nm, which is characteristic of zinc-metalated porphyrins.

Synthesis of the unsymmetrical dyad **4** was carried out in a similar fashion, except that in the initial step cyanuric chloride was left to react with Zn[TPP-NH_2] at 0 °C to give the metalated monoporphyrin triazine adduct. The free-base porphyrin was introduced in the following substitution reaction with H_2[TPP-NH_2], which was carried out at room temperature. Glycine methyl ester substitution at 65 °C gave compound **3**, which after basic hydrolysis resulted in the formation of dyad **4**. ^{1}H NMR, UV−vis absorption spectroscopy, and MALDI-TOF spectrometry confirmed the purity and identity of **4**. In the ^{1}H NMR spectrum of **4**, it is worth noting the absence of any signal due to the pyrrolic hydrogen atoms of the free-base porphyrin, which is attributed to H/D exchange, because a $CDCl_3$/MeOD = 1/0.01 mixture was used in order to increase the solubility.

Photophysical Properties. The UV−vis absorption spectra of **2** and **4** in solution (0.3 mM in $CHCl_3$/EtOH = 1/1) are shown in black in parts a and b of Figure 1a, respectively. Both compounds exhibit typical porphyrin absorption bands, with an intense Soret band in the 400−450 nm range and moderate Q bands in the 540−600 nm range. The Soret bands are broadened and split into doublets, which suggests intermolecular exciton coupling between porphyrin units of different dyads in their excited S_2 states.[32] The split Soret bands may also be caused by lowered molecular symmetry. The Q bands show large molar absorption coefficients (nearly double those of the monomeric porphyrin units) and no other additional spectral features, which may be attributed to the negligible interaction of the porphyrin units in their S_1 states.[16,33] The stronger Q bands should be related to lessened configuration interactions caused by lowered molecular symmetry.[8] The additional band observed in the case of the unsymmetrical dyad **4** at 552 nm may be assigned to the higher vibrational $Q_{1,0}$ band of the free-base porphyrin.

The UV−vis absorption spectra of **2** and **4** adsorbed onto TiO_2 films of 8 μm thickness are shown in parts a and b of Figure 1 (red color), respectively. Both dyads exhibit the usual Soret- and Q-band absorptions, but compared to their solution

dx.doi.org/10.1021/ic400774p | *Inorg. Chem.* 2013, 52, 9813−9825

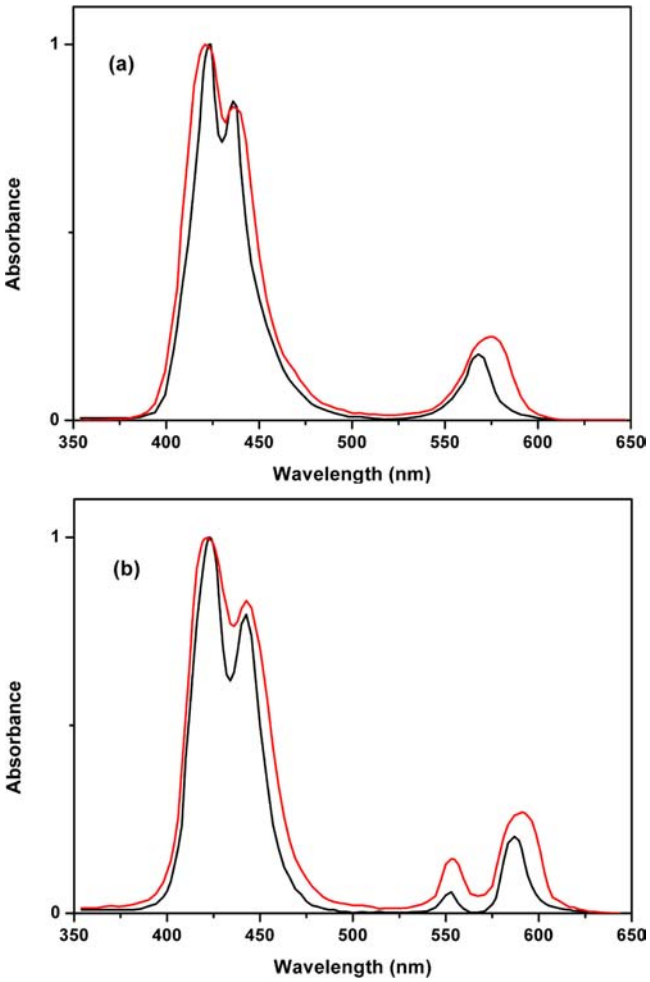

Figure 1. Normalized UV−vis absorption spectra of (a) **2** and (b) **4** in a $CHCl_3$/EtOH solution (black) and adsorbed onto a TiO_2 films (red).

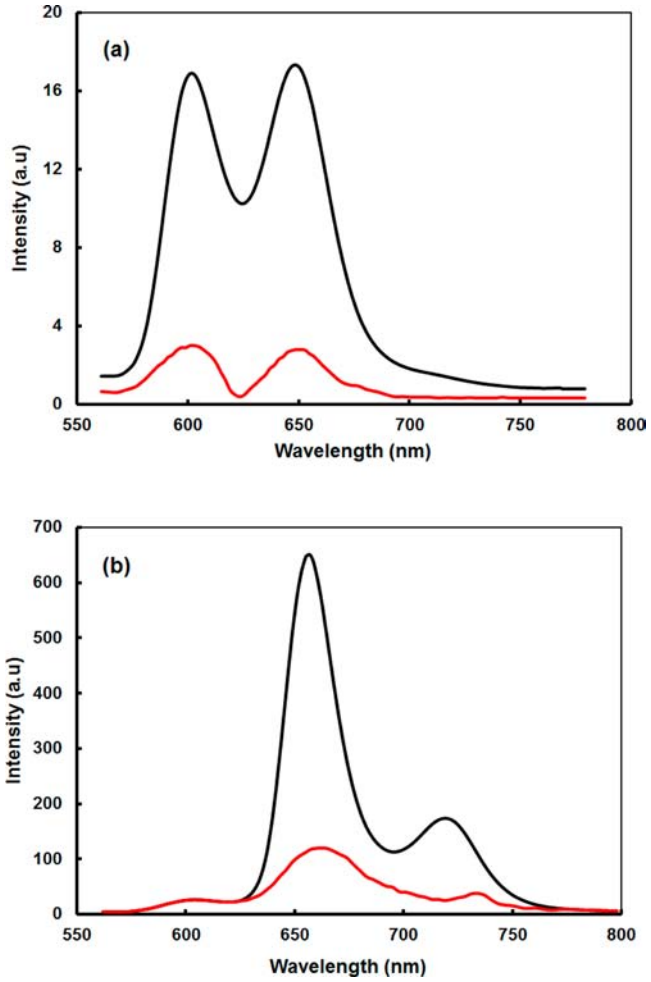

Figure 2. Fluorescence spectra of (a) **2** and (b) **4** in isoabsorbing CH_2Cl_2 solutions (black) and after their adsorption on TiO_2 (red).

spectra, these are much broader and shifted. Generally, when porphyrins are anchored onto the TiO_2 surface, they form either H aggregates, which result in broader Soret bands shifted to shorter wavelengths (blue shift) relative to their solution spectra, or J aggregates, which give sharp Soret bands shifted to longer wavelengths (red shift). The broader and blue-shifted Soret bands of **2** and **4** provide an indication of H-type aggregation for the porphyrin dimers on the TiO_2 surfaces.[34] The broadness and red shift of the Q bands is a sign of enhanced light-harvesting capacity to longer wavelengths of the solar spectrum of the two dyads.

On the basis of the onset absorption edge λ_{onset} of the Q bands of **2** and **4** on thin TiO_2 films and using the expression $E_g^{opt} = 1240/\lambda_{onset}$, the optical band gaps of **2** and **4** were calculated as 2.08 and 2.02 eV, respectively.

The steady-state fluorescence spectra of **2** and **4** in CH_2Cl_2 solutions and after their adsorption on TiO_2 are depicted in parts a and b of Figure 2, respectively. In solution, excitation of the two dyads at 422 nm (Soret band) results in photoluminescence, with two weak peaks of equal intensity at 603 and 650 nm for **2** and a strong peak at 655 nm and a moderate peak at 720 nm for **4** (black). After adsorption of **2** and **4** onto TiO_2, the fluorescence intensities for both dyes are reduced, providing significant quenching (red). This fluorescence quenching can be attributed to a photoinduced electron-transfer process from the zinc-metalated porphyrin units (which act as electron donors) to the TiO_2 surface.[35]

Electrochemical Studies. The electrochemical properties of dyads **2** and **4** were investigated by cyclic voltammetry measurements. The cyclic voltammograms of both compounds in THF are depicted in Figures S1 and S2 in the Supporting Information). Both compounds exhibit two oxidation waves at $E_{ox}^1 = +1.16$ V (quasi-reversible) and $E_{ox}^2 = +1.50$ V vs NHE for **2** and $E_{ox}^1 = +1.16$ V (quasi-reversible) and $E_{ox}^2 = +1.49$ V vs NHE for **4** (Table S1 in the Supporting Information). Furthermore, dyad **2** exhibits one reduction process at $E_{red}^1 = -1.13$ V vs NHE (quasi-reversible), while for **4**, there are two reduction processes at $E_{red}^1 = -0.89$ V (quasi-reversible) and $E_{red}^2 = -1.13$ V vs NHE. These data give an indication of negligible electronic interaction between the two porphyrin moieties in the ground states of the dyads.

The electrochemical properties of the methyl ester analogues of the carboxylic acid dyads **2** and **4**, compounds **1-Zn$_2$** and **3**, were also investigated. The cyclic voltammogram of the symmetrical dyad **1-Zn$_2$** in CH_2Cl_2 exhibits two oxidation and two reduction waves, while that of **3** shows four oxidation and three reduction waves (Figures S3−S5 and Table S2 in the Supporting Information). These are due to the usual stepwise oxidations and reductions by two electrons of the π-ring system of the porphyrin units of the dyads and not due to electronic interaction between the two porphyrin moieties of the dyads.

dx.doi.org/10.1021/ic400774p | Inorg. Chem. 2013, 52, 9813−9825

The additional irreversible oxidation and reduction processes observed in the voltammogram of **3** might be attributed to triazine moiety chemical side reactions.

For a sensitizer used for DSSC, suitable highest occupied molecular orbital (HOMO) and lowest unoccupied molecular orbital (LUMO) energy levels are required to enable efficient dye regeneration and electron injection processes. The HOMO and LUMO energies correspond to the first oxidation potential E_{ox} and first reduction potential E_{red} of the sensitizer, respectively. In order to ensure efficient electron injection from the photoexcited sensitizer into the TiO_2 conduction band (CB), the LUMO energy level of the sensitizer (E_{red}) should be higher than the TiO_2 CB edge (−0.5 V vs NHE). In addition, for efficient electron regeneration of the sensitizer radical cation (after photoinduced electron injection), the HOMO energy level of the sensitizer (E_{ox}) should be lower than the potential of the electrolyte redox I^-/I_3^- couple (+0.4 V vs NHE).[36] As shown in Figure 3, in which the

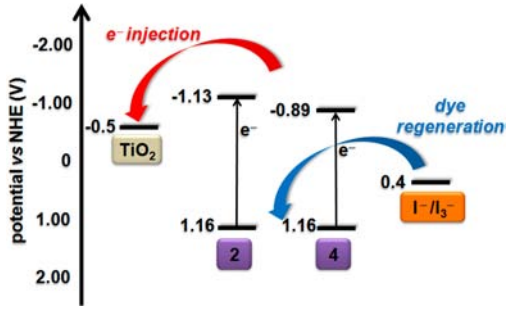

Figure 3. Electrochemical potential diagram showing the electron flow in **2**- and **4**-based DSSCs.

electrochemical potential data of **2**, **4**, the TiO_2 CB edge, and the I^-/I_3^- couple are depicted, the reduction potentials E_{red} of **2** and **4** are more negative than that of the TiO_2 CB edge and hence electron injection from the photoexcited dyads into the TiO_2 CB is thermodynamically favored (Table 1; $\Delta G_{inj} < 0$). In addition, their oxidation potentials (E_{ox}) are more positive than the redox potential of the I^-/I_3^- couple, which means that electron acceptance of the oxidized dyads from the electrolyte I^-/I_3^- couple is thermodynamically feasible (Table 1; $\Delta G_{reg} < 0$). Consequently, there is sufficient driving force for regeneration of the oxidized dyads **2** and **4** in DSSCs.

The HOMO−LUMO band gaps of **2** and **4** calculated from these electrochemical data are found to be 2.29 and 2.05 eV, respectively (Table 1). These are larger than the optical band gaps estimated from the photophysical measurements, but this is a common feature for organic dyes of this type, which can be attributed to solvent effects.[37]

In both **2** and **4**, the two porphyrin moieties, bridged by a triazine group, are nearly perpendicular to each other. In addition, **2** consists of two zinc-metalated porphyrin units, while **4** consists of a zinc-metalated and a free-base porphyrin unit. This structural difference may cause the difference in the HOMO and LUMO energy levels for each porphyrin moiety, favoring energy transfer to take place between the two moieties and toward the carboxylic acid group,[38] when dyad is excited with solar radiation.

DFT Calculations. To gain further insight into the electronic properties of **2** and **4**, DFT calculations at the B3LYP/6-31G level of theory were performed. The gas-phase geometry-optimized structures of the dyads are shown in Figure 4, while their optimized coordinates are provided in Tables S3

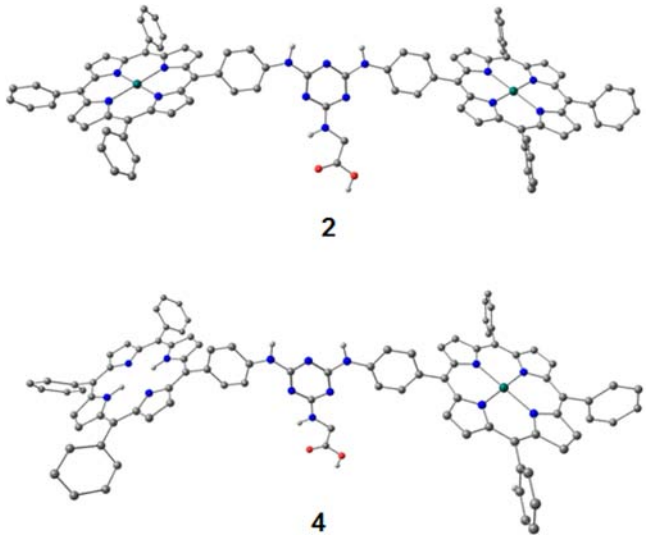

Figure 4. Geometry-optimized structures of **2** and **4** in the gas phase.

and S4 (Supporting Information), respectively. Both compounds exhibit a "butterfly-like" structure, in which the porphyrin units are attached in a perpendicular fashion to the triazine frame and they are slightly twisted against each other.

The electronic density distributions in the frontier orbitals of **2** and **4** are presented in Figure 5. In both dyads, no delocalization of the electronic density is observed along the two porphyrin units and the π-conjugated triazine linker, which suggests a very weak electronic communication between the two porphyrin units. This is an immediate consequence of the structures of the two dyads, in which the two porphyrin units are not coplanar with the triazine frame. HOMO and HOMO−1 of the symmetrical dyad **2** (Figure 5a) have very similar energies, and their electron densities are delocalized over both zinc-metalated porphyrins but unequally distributed (mainly on

Table 1. Electrochemical Data and Calculated HOMO and LUMO Energy Levels, Band Gaps, and ΔG Values for Electron Injection and Regeneration Processes for 2 and 4

compound	$E_{ox}{}^a$/V	$E_{red}{}^a$/V	HOMO^b/eV	LUMO^b/eV	band gap^b/eV	$\Delta G_{inj}{}^c$/eV	$\Delta G_{reg}{}^c$/eV
2	1.16	−1.13	−5.56	−3.27	2.29	−0.63	−0.76
4	1.16	−0.89	−5.56	−3.51	2.05	−0.39	−0.76

[a]Observed first oxidation and reduction potentials (vs NHE). [b]HOMO and LUMO energy levels and band gaps calculated according to the relationships $E_{HOMO} = -(E_{ox} + 4.4)$ eV and $E_{LUMO} = -(E_{red} + 4.4)$ eV, measured with reference to the redox potential −4.4 eV. [c]ΔG_{inj} for electron injection from the LUMO of the dyads to the TiO_2 CB (−0.5 V vs NHE) and ΔG_{reg} for regeneration of the dyad radical cations by the I^-/I_3^- redox couple (0.4 V vs NHE).

dx.doi.org/10.1021/ic400774p | Inorg. Chem. 2013, 52, 9813−9825

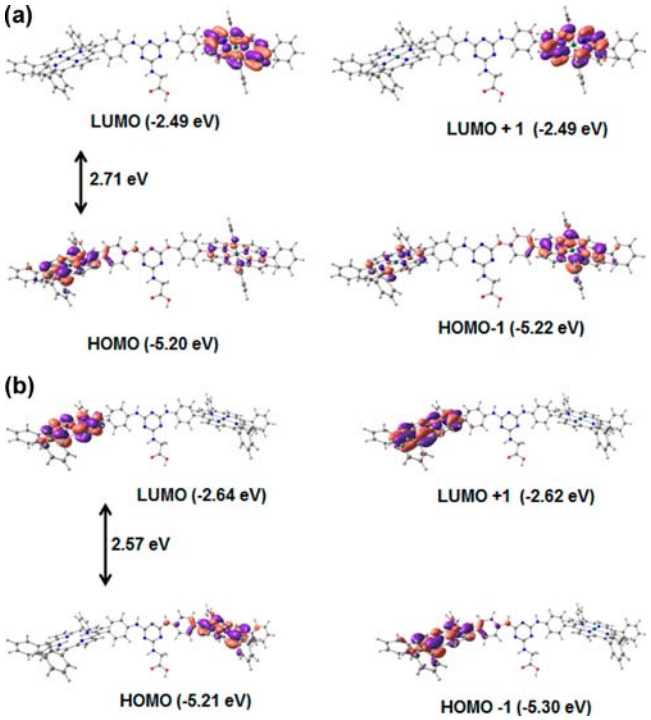

Figure 5. Frontier molecular orbitals of (a) **2** and (b) **4** and corresponding energy levels from DFT calculations in CH_2Cl_2.

one of the zinc-metalated porphyrins), whereas LUMO and LUMO+1 are degenerate and the electron density is localized on one of the zinc-metalated porphyrins. For the unsymmetrical dyad **4** (Figure 5b), the HOMO electron density is localized only on the zinc-metalated porphyrin, while LUMO and LUMO+1 are almost degenerate and the electron density is localized only on the free-base porphyrin. Considering that a zinc-metalated porphyrin acts as an electron donor (D) and a free-base porphyrin unit as an electron acceptor (A), the dyads **2** and **4** can be described as D−π−D and D−π−A systems, respectively, where π denotes the triazene−π system. It should be noted that, for efficient application of a sensitizer in a DSSC, in order to have a successful electron injection into the TiO_2 CB, the LUMO electron density of the sensitizer should be localized on (or close to) A, which is usually the anchoring group. However, in both dyads, the LUMO is localized on one of the porphyrin units and not on the anchoring carboxylic acid group of the glycine moiety.

The HOMO−LUMO gap of **2** is estimated to be 2.71 eV, which is close to the value of 2.29 eV, calculated from the experimentally observed oxidation E_{ox} and reduction potentials E_{red} (Table 2). Similarly, the theoretically estimated HOMO−LUMO gap of **4** in a CH_2Cl_2 solution is in good agreement with the experimental value.

TDDFT calculations have been an important tool for the prediction of electronic transitions for many types of molecules. This method has been extensively used for simulating the absorption spectra, as well as for assigning the spectral transitions, of porphyrins.[39] In order to obtain deeper insight into the electronic transitions of **2** and **4**, TDDFT calculations were carried out in CH_2Cl_2 as the solvent medium. The calculation for the symmetrical dyad **2** with two zinc-metalated porpyrin units revealed two closely spaced intense peaks at 395.7 nm (f = 1.73) and 395.6 nm (f = 1.95) (Figure 6a),

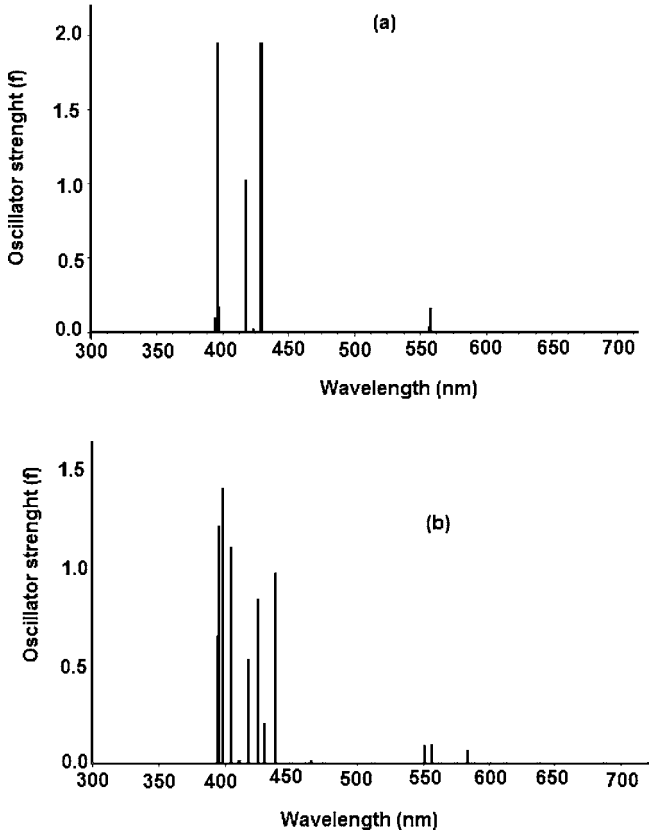

Figure 6. TDDFT-calculated vertical transitions of (a) **2** and (b) **4** in CH_2Cl_2.

which involve contributions primarily from HOMO−3 → LUMO, HOMO−2 → LUMO+2, HOMO−2 → LUMO+3, and HOMO−3 → LUMO+1 and correspond to the π−π^* transitions of the zinc-metalated porphyrin Soret band. The vertical transitions calculated at 557.2 nm (f = 0.1665) and 556.2 nm (f = 0.045) correspond to the Q-band transitions of the zinc porphyrin units. These are π−π^* transitions that have primary contributions from HOMO → LUMO+3 and HOMO−2 → LUMO+2 transitions.

In the case of **4**, a larger number of peaks are observed than those in **2** in the Soret-band as well as in the Q-band regions (Figure 6b), presumably because of its asymmetrical structure (which consists of a free-base porphyrin and a zinc-metalated

Table 2. Calculated HOMO and LUMO Levels and Band Gaps from DFT Calculations in the Solution Phase and Electrochemical Data for 2 and 4

compound	HOMO[a]/eV	LUMO[a]/eV	band gap[a]/eV	HOMO[b]/eV	LUMO[b]/eV	band gap[b]/eV
2	−5.56	−3.27	2.29	−5.20	−2.49	2.71
4	−5.56	−3.51	2.05	−5.21	−2.64	2.57

[a]Calculated from electrochemical data. [b]Estimated from DFT calculations in the solution phase.

dx.doi.org/10.1021/ic400774p | Inorg. Chem. 2013, 52, 9813−9825

Table 3. Photovoltaic Parameters of 2- and 4-Based DSSCs

compound	J_{sc}[a]/(mA/cm^2)	V_{oc}[b]/V	FF[c]	PCE[d]/%	dye loading/(mol/cm^2)	τ_e[e]/ms	τ_d[f]/ms	η_{cc}[g]
2	8.82	0.63	0.65	3.61	2.42×10^{-6}	16	12	0.57
4	9.94	0.66	0.68	4.46	2.68×10^{-6}	24	8	0.75

[a]Short-circuit current. [b]Open-circuit voltage. [c]Fill factor. [d]Photoconversion efficiency. [e]Electron lifetime. [f]Electron-transport time. [g]Charge collection efficiency calculated by $\eta_{cc} = [1 + (\tau_d/\tau_e)]^{-1}$ (photoanode = TiO_2 of 10 μm thickness).

porphyrin unit). The asymmetrical structure of **4** is also evident by its calculated dipole moment of 2.1762 D, which is higher than that of the symmetrical dyad **2** (1.8696 D). The observed peaks at 404.3 nm (f = 1.11) and 397.8 nm (f = 1.41) have major contributions from HOMO−3 → LUMO+1, HOMO−3 → LUMO, and HOMO−1 → LUMO+1 and can be assigned to $\pi-\pi^*$ transitions of the free-base porphyrin unit Soret band. Another peak at 395.2 nm (f = 1.21), consisting of transitions from HOMO → LUMO+2, HOMO−2 → LUMO+2, and HOMO → LUMO+3, can be assigned to the Soret band of the zinc porphyrin unit. The calculated Q-band peaks are observed at 583.8, 556.4, 556.2, and 550.4 nm and can be attributed to $\pi-\pi^*$ transitions of the two porphyrin moieties.

FTIR Spectra. The triazine group of the dyads **2** and **4** is functionalized by a carboxylic acid of a glycine moiety, as the anchoring group for attachment onto the TiO_2 surface of electrodes of solar cells. To get information about the anchoring of **2** and **4** onto the TiO_2 surface, FTIR powder spectra of **2** and **4**, in pure form and adsorbed onto TiO_2 films, were recorded (representative FTIR spectra of **2** and **2** absorbed onto TiO_2 are shown in Figure S12 in the Supporting Information). Both dyads in pure form exhibit very strong absorption peaks at 1687 cm^{-1}, which correspond to the ν(CO) stretching vibrations of the carboxylic acid groups. In the corresponding spectra of the dyad/TiO_2 films, these peaks are shifted to lower frequencies at 1645 and 1414 cm^{-1} [assigned as $\nu_{asym}(COO^-)$ and $\nu_{sym}(COO^-)$, respectively], which is a sign of the strong binding and electronic coupling of **2** and **4** through their carboxylic acid groups on the TiO_2 surface.[40]

Photovoltaic Performance. **2**- and **4**-based DSSCs have been fabricated, and their photovoltaic cell parameters are summarized in Table 3. Their current−voltage ($J-V$) curves and the corresponding IPCE spectra are shown in parts a and b of Figure 7, respectively. The **4**-based solar cell yields a PCE value of 4.46%, while the **2**-based solar cell gives a lower value of 3.61%. This difference can be primarily attributed to the enhanced short-circuit current J_{sc} and second to the higher open-circuit voltage V_{oc} and fill factor FF values of the **4**-based cell.

The higher J_{sc} value for DSSC based on the **4** dye is consistent with its larger IPCE value. The IPCE values at wavelength 590 nm of **2**- and **4**-sensitized DSSCs were found to be 43% and 51%, respectively (Figure 7b). IPCE is defined as

$$\text{IPCE} = \text{LHE} \times \eta_{inj}\eta_{cc}$$

where LHE is the light-harvesting efficiency (which depends on the absorption of the sensitized sensitizer), η_{inj} is the electron-injection efficiency (which depends on the electron-injection rate from the sensitizer into the TiO_2 CB), and η_{cc} is the charge collection efficiency (which depends on the diffusion rate of electrons in TiO_2 and the recombination rate between the electrons and redox couple of the electrolyte).

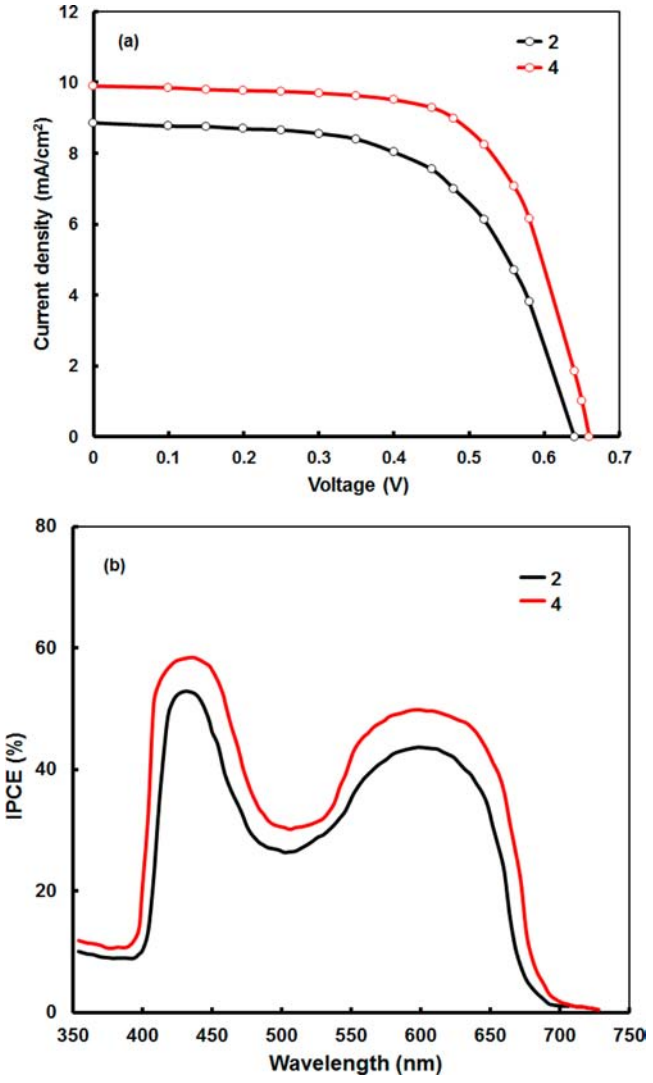

Figure 7. (a) Current−voltage ($J-V$) curves under illumination and (b) IPCE spectra of **2**- and **4**-based DSSCs.

Another critical factor in determining the PCE and IPCE values of a DSSC is the dye loading on the TiO_2 surface.[41] To obtain the dye loading value of the photoanode, the dye-sensitized TiO_2 layer was immersed into a mixture of CH_2Cl_2 and NaOH(aq). The total amounts of dye adsorbed onto the TiO_2 surface, i.e., dye loading, were obtained by measuring the absorption spectra of dissolved porphyrin in the mixture solvent. The dye loading values for **2** and **4** were found to be 2.42×10^{-6} and 2.68×10^{-6} mol/cm^2, respectively. The IPCE value is dominated by LHE = $(1 - 10^{-abs})$, for which the absorbance (abs) is linearly dependent on both the dye loading on TiO_2 and absorption coefficient. The IPCE values at both Soret and Q bands are larger for **4** than **2**. As shown in the absorption spectra of porphyrin/TiO_2 (Figure 1a,b) and dye loading values, the LHE of the **4**-based cell is larger than that

dx.doi.org/10.1021/ic400774p | Inorg. Chem. 2013, 52, 9813−9825

for **2**. We assume that, in addition to a larger amount of dye loading to give larger LHE for **4**, the possibility of a lower TiO_2 CB edge upon dye uptake of the **4**-based DSSC might lead to a larger injection rate to give a higher electron yield for this device. This may also be related to the formation of a blocking layer caused by the higher dye loading.[42]

In general, the V_{oc} value is determined by the difference between the Fermi level of electrons in TiO_2 and the redox potential level of a redox couple in the electrolyte. Because the potential levels of the redox couples in these devices are the same, the value of V_{oc} depends on the Fermi levels for electrons after electron injection in both porphyrin systems. The V_{oc} value of the DSSC can be determined from the expression[43]

$$V_{oc} = \left(\frac{E_{CB}}{q}\right) + \left(\frac{kT}{q}\right)\ln\left(\frac{n_c}{N_{CB}}\right) - \left(\frac{E_{red}}{q}\right)$$

where E_{CB} is the TiO_2 CB edge, E_{red} is the electrolyte redox potential, kT represents the thermal energy, and n_c and N_{CB} are the number of electrons and density of states in the TiO_2 CB, respectively. After adsorption of the dye on the TiO_2 surface, a shift of E_{CB} takes place and ΔE_{CB} is given by the expression[43]

$$\Delta E_{CB} = \frac{-q\mu_{normal}\gamma}{\varepsilon_0\varepsilon}$$

where μ_{normal} represents the dipole moment of the adsorbed dye vertical to the TiO_2 surface, γ is the concentration of dye molecules adsorbed on the TiO_2 surface (dye loading), and ε_0 and ε are the permittivity of the dye under vacuum and dielectric constant on the dye monolayer, respectively. From the above equation, it is apparent that a dye with large μ_{normal} and γ yields high V_{oc}. Because the dipole moment of **4** is larger than that of **2** and the **4**-based solar cell exhibits higher dye loading, then ΔE_{CB} is larger for the **2**-based DSSC and consequently the **4**-based DSSC is expected to result in a higher V_{oc} value.

On the basis of the $J-V$ characteristics obtained in the dark (Figure S13 in the Supporting Information), the DSSC based on **4** shows a lower current than the **2**-sensitized DSSC. Because of the fact that the dark current density is governed by the impedance of the electron recombination between TiO_2 and the electrolyte impedance of the electron recombination between TiO_2 and the electrolyte governs the dark current density, the adsorbed porphyrin dye molecules on TiO_2 might play a role, by increasing the interfacial impedance depending upon the degree of coverage of sensitizing dye on the surface of TiO_2. According to the results of dye loading, the larger dye loading on the TiO_2 surface in the **4**-based DSSC behaves like a blocking layer, which prevents charge recombination between TiO_2 and I_3^- of the electrolyte. However, for **2**, which has a lower surface coverage on the TiO_2 surface, I_3^- in the electrolyte can penetrate closely to the surface of TiO_2 to decrease the barrier for electrons to recombination with I_3^- and to result in a higher dark current.

From the above, it is evident that both dyads **2** and **4** can act as efficient sensitizers for DSSCs. However, the PCE values reported herein are lower than those reported for DSSCs sensitized by "push−pull" multiporphyrin arrays.[44] The reason for this difference lies on the different electron structures of the sensitizers. The structure of a "push−pull" is a D−π−A system, with the anchoring group residing on A, which results in very effective electron flow into the TiO_2 CB. The structures of dyads **2** and **4** presented herein are described as D−π−D and D−π−A, respectively, with their anchoring group located on the π linker. As a result, although triazine mediates effectively intramolecular electron-transfer and charge-separation phenomena between the porphyrin units in the dyads and promotes electron injection into the TiO_2 electrode, the electron flow is not as efficient as that in the "push−pull" systems.

The larger PCE value of the **4**-based solar cell can be attributed to its unsymmetrical structure with respect to the symmetrical structure of **2**, which consists of two identical zinc-metalated porphyrin units. Asymmetry has been proposed as the reason for increased efficiency of solar cells sensitized by other porphyrin dyads[17] as well as other non-"push−pull" porphyrins.[13,45] The completely symmetrical system of **2** provides no directionality for the electron-transfer process. However, in the case of the unsymmetrical system of **4**, the presence of both zinc-metalated and free-base porphyrin units causes a polarizing and cooperating effect, directing electron transfer toward TiO_2 and therefore leading to more efficient electron-injection process.

In order to gain a better understanding of the observed photovoltaic parameters of **2**- and **4**-based DSSC properties, EIS was performed to analyze the effects on charge generation, transport, and collection.[46] Figure 8 depicts the EIS spectra of **2**- and **4**-based DSSCs, in the dark under a forward bias of 0.65 V. In general, the Nyquist plots of EIS spectra in the dark, in the frequency range 0.1−10 kHz, show three semicircles. The semicircle radius in the high-frequency range (left side of the spectrum) represents the charge-transfer resistance at the

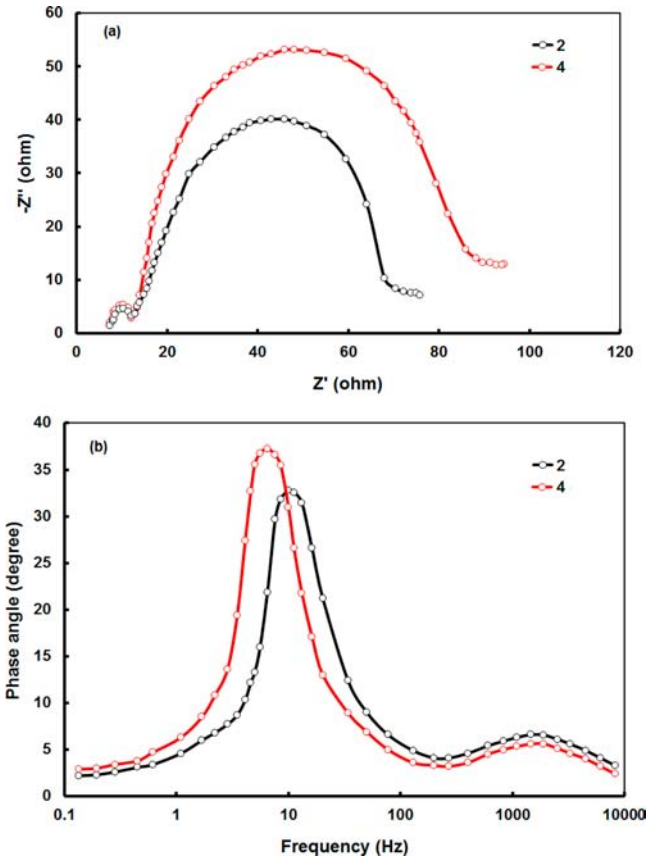

Figure 8. EIS spectra of (a) Nyquist and (b) Bode plots of **2**- and **4**-based DSSCs, measured at a bias voltage of 0.65 V under dark conditions.

dx.doi.org/10.1021/ic400774p | Inorg. Chem. 2013, 52, 9813−9825

counter electrode/electrolyte interface. The charge recombination resistance at TiO_2/dye/electrolyte corresponds to the semicircle in the middle-frequency range. In the low-frequency range, the impedance is associated with the Warburg diffusion process of I^-/I_3^- in the electrolyte. As can be seen in Figure 8a, the semicircle radius in the middle-frequency range is larger for the DSSC based on **4** compared to **2**, indicating that the charge recombination rate is slower for the former device.

The electron lifetime was calculated from the peak frequency (f_{peak}) at the intermediate-frequency region in a Bode phase plot (Figure 8b) according to $\tau_e = 1/2\pi f_{peak}$. The electron lifetimes for the DSSCs based on **2** and **4** are 16 and 24 ms, respectively, indicating that the charge recombination is suppressed for **4**, compared to **2**. The higher electron lifetime for **4** relative to that of **2** could be attributed to the D−π−A nature of **4**, which disturbs the dispersion forces by trapping I_3^- near the porphyrin more effectively, preventing the approach of I_3^- to the linker group and the surface region. In this case, the distance from the surface of TiO_2 to the trapped I_3^- is expected to be longer than the distance between the surface and the I_3^- attached to the conjugated linker of **2**, explaining the longer electron lifetime of DSSC based on **4** compared to **2**. In contrast, **2**, which behaves as a D−D porphyrin dye, could increase the surface I_3^- concentration by attracting the acceptor to its linker through dispersion forces, leading to a shorter electron lifetime and increasing the back-recombination of injected electrons in TiO_2.[47]

To get the more information about the charge-transport mechanism in the DSSCs, we have also performed EIS measurements under illumination at the bias voltage of 0.65 V, and the Nyquist plots for DSSCs based on **2** and **4** are shown in Figure 9. The semicircle in the intermediate-

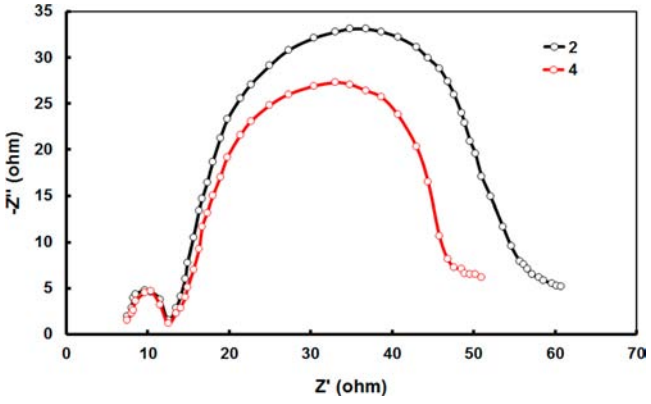

Figure 9. Nyquist plots of EIS spectra measured at a bias voltage of 0.65 V under illumination, for **2**- and **4**-based DSSCs.

frequency region corresponds to the charge-transport mechanism at the TiO_2/dye/electrolyte interface after photoexcitation. The diameter of this semicircle is the measure of the charge-transport resistance (R_{tran}). It can be seen that the diameter of this semicircle is smaller for the DSSC sensitized with **4** than that for **2**, resulting in a low value of R_{tran}, indicating fast transport of electrons in the TiO_2 layer toward the FTO electrode. The electron-transport time (τ_d) of an injected electron in the TiO_2 film is related with τ_e, R_{rec}, and R_{tran} as follows:[48]

$$\frac{\tau_d}{\tau_e} = \frac{R_{tranr}}{R_{rec}}$$

The values of the electron lifetime and electron-transport time are listed in Table 3. The electron-transport time is a measure of the average time taken for the collection of injected electrons, and a faster electron-transport time is associated with a higher photocurrent because it indicates that the electrons hop across the TiO_2 network and are collected at the photoanode at a faster rate.[49] The decrease in R_{tran} and the increase in R_{rec} for the DSSC sensitized with **4** indicate that the electron-transport time has decreased for the DSSC based on **4**. This means that the electrons are reaching the FTO substrate in the DSSC sensitized with **4** faster than they are with **2** because the electron-transport rate is enhanced.

Furthermore, the photovoltaic performance was evidently reflected by the charge collection efficiencies $\eta_{cc} = [1 + (\tau_d/\tau_e)]^{-1}$,[50] the values of which were found to be 0.57 and 0.75 for DSSCs sensitized with **2** and **4**, respectively (Table 3). A higher charge collection efficiency value leads to an improved PCE value in the case of the **4**-based DSSC.

CONCLUSIONS

In summary, we have synthesized two novel porphyrin−porphyrin dyads, the symmetrical Zn[Porph]−Zn[Porph] (**2**) and unsymmetrical Zn[Porph]−H_2[Porph] (**4**), which are covalently linked through arylamino groups at their peripheries by 1,3,5-triazine, by taking advantage of the stepwise and temperature-dependent reactivity of cyanuric chloride. The dyads are also functionalized by a terminal carboxylic acid group of a glycine moiety attached to the triazine group. The study of the photophysical and electronic properties of the two compounds revealed not significant electronic interaction in their ground states but broadened spectral absorptions and suitable frontier orbital energy levels for use in DSSCs. **2**- and **4**-based DSSCs were fabricated, demonstrating efficient intramolecular electron-transfer and charge-separation phenomena mediated by the triazine group and PCE values of 3.61% and 4.46%, respectively. The higher PCE value of the **4**-based DSSC is attributed to its larger dye loading and higher J_{sc}, V_{oc}, and FF values. On the basis of the DFT results, the unsymmetrical structure of **4** does not have localized frontier molecular orbital patterns, but the direction of the HOMO/LUMO pattern shifts is not aligned with that of electron injection. The $J-V$ curves of the two cells as well as their IPCE and EI spectra demonstrated enhancement of the short-circuit current (J_{sc}) under illumination for the **4**-based DSSC, due to shorter electron-transport time (τ_d), longer electron lifetime (τ_e), and high charge recombination resistance, as well as larger dye loading onto the TiO_2 surface. Further improvement of the PCE values of DSSCs reported herein may be achieved by using a modified photoanode, and we are currently working in this direction.

ASSOCIATED CONTENT

Supporting Information

Complementary data of cyclic voltammograms, ^1H and ^{13}C NMR spectra of compounds **1**, **1-Zn$_2$**, **2**, **3**, and **4**, FTIR spectra of **2** and **2** absorbed on TiO_2, dark current-voltage characteristics of **2**- and **4**-based DSSCs, and optimized coordinates from DFT calculations for **2** and **4**. This material is available free of charge via the Internet at http://pubs.acs.org.

dx.doi.org/10.1021/ic400774p | Inorg. Chem. 2013, 52, 9813−9825

AUTHOR INFORMATION

Corresponding Author

*E-mail: coutsole@chemistry.uoc.gr (A.G.C.), gdsharma273@gmail.com (G.D.S.).

Notes

The authors declare no competing financial interest.

ACKNOWLEDGMENTS

Financial support from the European Commission (FP7-REGPOT-2008-1, Project BIOSOLENUTI No. 229927) is greatly acknowledged. This research has also been cofinanced by the European Union (European Social Fund) and Greek national funds (Heraklitos II) through the Operational Program "Education and Lifelong Learning" of the National Strategic Reference Framework Research Funding Program (THALIS-UOA-MIS 377252).

REFERENCES

(1) (a) O'Regan, B.; Grätzel, M. *Nature* **1991**, *353*, 737. (b) Grätzel, M. *Acc. Chem. Res.* **2009**, *42*, 1788. (c) Hagfeldt, A.; Boschloo, G.; Sun, L.; Kloo, L.; Pettersson, H. *Chem. Rev.* **2010**, *110*, 6595.

(2) Liska, L.; Cevey, E.; Costa, V.; Shklover, L.; Spiccia, G. B.; Deacon, C. A.; Bignozzi, M.; Grätzel, M. *J. Am. Chem. Soc.* **2001**, *123*, 1613.

(3) (a) Chiba, Y.; Islam, A.; Watanabe, Y.; Komiya, R.; Koide, N.; Han, L. *Jpn. J. Appl. Phys.* **2006**, *45*, L638. (b) Nazeeruddin, M. K.; Pechy, P.; Renouard, T.; Zakeeruddin, S. M.; Hymphry-Baker, R.; Comte, P.; Nazeeruddin, P. L. M. K.; De Angelis, F.; Fantacci, S.; Selloni, A.; Viscardi, G.; Liska, P.; Ito, S.; Takeru, B.; Grätzel, M. *J. Am. Chem. Soc.* **2005**, *127*, 16835−16847. (c) Gao, F.; Wang, Y.; Shi, D.; Zhang, J.; Wang, M.; Jing, X.; Humphry-Baker, R.; Wang, P.; Zakeeruddin, S.; Grätzel, M. *J. Am. Chem. Soc.* **2008**, *130*, 10720. (d) Chen, C.; Wang, M.; Li, J.; Pootrakulchote, N.; Alibabaei, L.; Ngoc-le, C.; Decoppet, J.-D.; Tsai, J. H.; Grätzel, C.; Wu, C.-G.; Zakeeruddin, S. M.; Grätzel, M. *ACS Nano* **2009**, *3*, 3103. (e) Wang, Q.; Ito, S.; Grätzel, M.; Fabregat-Santiago, F.; Mora-Sero, I.; Bisquert, J.; Bessho, T.; Imai, H. *J. Phys. Chem. B* **2006**, *110*, 25210. (f) Cao, Y. M.; Bai, Y.; Yu, Q. J.; Cheng, Y. M.; Liu, S.; Shi, D.; Gao, F. F.; Wang, P. *J. Phys. Chem. C* **2009**, *113*, 6290. (g) Yu, Q. J.; Wang, Y. H.; Yi, Z. H.; Zu, N. N.; Zhang, J.; Zhang, M.; Wang, P. *ACS Nano* **2010**, *4*, 6032. (h) Han, L. Y.; Islam, A.; Chen, H.; Malapaka, C.; Chiranjeevi, B.; Zhang, S. F.; Yang, X. D.; Yanagida, M. *Energy Environ. Sci.* **2012**, *5*, 6057.

(4) (a) Mishra, A.; Fischer, M. K. R.; Beuerle, P. *Angew. Chem., Int. Ed.* **2009**, *48*, 2474 and references cited therein. (b) Ooyama, Y.; Harima, Y. *Eur. J. Org. Chem.* **2009**, 2903. (c) Ooyama, Y.; Harima, Y. *Chem. Phys. Chem.* **2012**, *13*, 4032 and references cited therein.

(5) (a) Im, H.; Kim, S.; Park, C.; Jang, S. H.; Kim, C. J.; Kim, K.; Park, N. G.; Kim, C. *Chem. Commun.* **2010**, *46*, 1335. (b) Zeng, W.; Cao, Y.; Bai, Y.; Wang, Y.; Shi, Y.; Zhang, M.; Wang, F.; Pan, C.; Wang, P. *Chem. Mater.* **2010**, *22*, 1915.

(6) (a) Ito, S.; Nazeeruddin, M. K.; Liska, P.; Comte, P.; Charvet, R.; Pechy, P.; Jirousek, M.; Kay, A.; Zakeeruddin, S. M.; Grätzel, M. *Prog. Photovoltaics* **2006**, *14*, 589. (b) Kroon, J. M.; Bakker, N. J.; Smit, H. J. P.; Liska, P.; Thampi, K. R.; Wang, P.; Zakeeruddin, S. M.; Grätzel, M.; Hinsch, A.; Hore, S. *Prog. Photovoltaics* **2007**, *15*, 1. (c) Green, M. A.; Emery, K.; King, D. L.; Hishikawa, Y.; Warta, W. *Prog. Photovoltaics* **2007**, *15*, 35.

(7) (a) Eu, S.; Hayashi, S.; Umeyama, T.; Matano, Y.; Araki, Y.; Imahori, H. *J. Phys. Chem. C* **2008**, *112*, 4396. (b) Cid, J.-J.; Yum, J.-H.; Jang, S.-R.; Nazeeruddin, M. K.; Martinez-Ferrero, E.; Palomares, E.; Ko, J.; Gratzel, M.; Torres, T. *Angew. Chem., Int. Ed.* **2007**, *46*, 8358. (c) Li, L.-L.; Diau, E. W.-G. *Chem. Soc. Rev.* **2013**, *42*, 291.

(8) Gouterman, M. *J. Mol. Spectrosc.* **1961**, *6*, 138.

(9) (a) Himahori, H.; Umeyama, T.; Ito, S. *Acc. Chem. Res.* **2009**, *42*, 1809. (b) Campbell, W. M.; Burrell, A. K.; Officer, D. L; Jolley, K. W. *Coord. Chem. Rev.* **2004**, *248*, 1363. (c) Martinez-Diaz, M. V.; de La Torre, G.; Torres, T. *Chem. Commun.* **2010**, *46*, 7090. (d) Ball, J. M.; Davis, N. K. S.; Wilkinson, J. D.; Kirkpatrick, J.; Teuscher, J.; Gunning, R.; Anderson, H. L.; Snaith, H. J. *RSC Adv.* **2012**, *2*, 6846.

(10) Campbell, W. M.; Jolley, K. W.; Wagner, P.; Wagner, K.; Walsh, P. J.; Gordon, K. C.; Schmidt-Mende, L.; Nazeeruddin, M. K.; Wang, Q.; Grätzel, M.; Officer, D. L. *J. Phys. Chem. C* **2007**, *111*, 11760.

(11) Bessho, T.; Zakeeruddin, S. M.; Yeh, C.-Y.; Diau, E. W.-G.; Grätzel, M. *Angew. Chem., Int. Ed.* **2010**, *49*, 6646.

(12) Yella, A.; Lee, H.-W.; Tsao, H. N.; Yi, C.; Chandiran, A. K.; Nazeeruddin, M. K.; Diau, E. W.-G.; Yeh, C.-Y.; Zakeeruddin, S. M.; Grätzel, M. *Science* **2011**, *334*, 629.

(13) (a) Wang, C.-L.; Chang, Y.-C.; Lan, C.-M.; Lo, C.-F.; Diau, E. W.-G.; Lin, C.-Y. *Energy Environ. Sci.* **2011**, *4*, 1788. (b) Wang, C.-L.; Lan, C.-M.; Hong, S.-H.; Wang, Y. F.; Pan, T.-Y.; Chang, C. W.; Kuo, H. H.; Kuo, M. Y.; Diau, E. W.-G.; Lin, C. Y. *Energy Environ. Sci.* **2012**, *5*, 6933.

(14) Koehorst, R. B. M.; Boschloo, G. K.; Savenije, T. J.; Goossens, A.; Schaafsma, T. J. *J. Phys. Chem. B* **2000**, *104*, 2371.

(15) Park, J. K.; Chen, J. P.; Lee, H. R.; Park, S. W.; Shinokubo, H.; Osuka, A.; Kim, D. *J. Phys. Chem. C* **2009**, *113*, 21956.

(16) Mozer, A. J.; Griffith, M. J.; Tsekouras, G.; Wagner, P.; Wallace, G. G.; Mori, S.; Sunahara, K.; Miyashita, M.; Earles, J. C.; Gordon, K. C.; Du, L. C.; Katoh, R.; Furube, A.; Officer, D. L. *J. Am. Chem. Soc.* **2009**, *131*, 15621.

(17) Dy, J. T.; Tamaki, K.; Sanehira, Y.; Nakazaki, J.; Uchida, S.; Kuba, T.; Segawa, H. *Electrochemistry* **2009**, *3*, 206.

(18) Ladomenou, K.; Lazarides, T.; Panda, M. K.; Charalambidis, G.; Daphnomili, D.; Coutsolelos, A. G. *Inorg. Chem.* **2012**, *51*, 10548.

(19) Kohn, W.; Sham, L. *J. Phys. Rev.* **1965**, *140*, A1133.

(20) Frisch, M. J.; Trucks, G. W.; Schlegel, H. B.; Scuseria, G. E.; Robb, M. A.; Cheeseman, J. R.; Montgomery, J. A., Jr.; Vreven, T.; Kudin, K. N.; Burant, J. C.; Millam, J. M.; Lyengar, S. S.; Tomasi, J.; Barone, V.; Mennucci, B.; Cossi, M.; Scalmani, G.; Rega, N.; Petersson, G. A.; Nakatsuji, H.; Hada, M.; Ehara, M.; Toyota, K.; Fukuda, R.; Hasegawa, J.; Ishida, M.; Nakajima, T.; Honda, Y.; Kitao, O.; Nakai, H.; Klene, M.; Li, X.; Knox, J. E.; Hratchian, H. P.; Cross, J. B.; Bakken, V.; Adamo, C.; Jaramillo, J.; Gomperts, R.; Stratmann, R. E.; Yazyev, O.; Austin, A. J.; Cammi, R.; Pomelli, C.; Ochterski, J. W.; Ayala, P. Y.; Morokuma, K.; Voth, G. A.; Salvador, P.; Dannenberg, J. J.; Zakrzewski, V. G.; Dapprich, S.; Daniels, A. D.; Strain, M. C.; Farkas, O.; Malick, D. K.; Rabuck, A. D.; Raghavachari, K.; Foresman, J. B.; Ortiz, J. V.; Cui, Q.; Baboul, A. G.; Clifford, S.; Cioslowski, J.; Stefanov, B. B.; Liu, G.; Liashenko, A.; Piskorz, P.; Komaromi, I.; Martin, R. L.; Fox, D. J.; Keith, T.; Al-Laham, M. A.; Peng, C. Y.; Nanayakkara, A.; Challacombe, M.; Gill, P. M. W.; Johnson, B.; Chen, W.; Wong, M. W.; Gonzalez, C.; Pople, J. A. *Gaussian 03*; Gaussian Inc.: Wallingford, CT, 2004.

(21) Lee, C. T.; Yang, W. T.; Parr, R. G. *Phys. Rev. B* **1988**, *37*, 785.

(22) Becke, A. D. *Phys. Rev. A* **1988**, *38*, 3098.

(23) Zhurko, D. A.; Zhurko, G. A. *ChemCraft 1.6*; Plimus: San Diego, CA, available at http://www.chemcraftprog.com.

(24) Cossi, M.; Barone, V.; Cammi, R.; Tomasi, J. *Chem. Phys. Lett.* **1996**, *255*, 327.

(25) Tomasi, J.; Mennucci, B.; Cammi, R. *Chem. Rev.* **2005**, *105*, 2999.

(26) Daphnomili, D.; Landrou, G.; Singh, S. P.; Thomas, A.; Yesudas, K.; Bhanuprakash, K.; Sharma, G. D.; Coutsolelos, A. G. *RCS Adv.* **2012**, *2*, 12899.

(27) (a) Blotny, G. *Tetrahedron* **2006**, *62*, 9507. (b) Chaleix, V.; Sol, V.; Krausz, P. *Tetrahedron Lett.* **2011**, *52*, 2977. (c) Ringot, C.; Saad, N.; Granet, R.; Bressollier, P.; Sol, V.; Krausz, P . *J. Porphyrins Phthalocyanines* **2010**, *14*, 925.

(28) Löwik, D. W. P. M.; Lowe, C. R. *Eur. J. Org. Chem.* **2001**, 2825.

(29) (a) Steffensen, M. B.; Simanek, E. E. *Org. Lett.* **2003**, *5*, 2359. (b) Zhang, W.; Simanek, E. E. *Org. Lett.* **2000**, *2*, 843.

(30) (a) Carofiglio, T.; Varotto, A.; Tonellato, U. *J. Org. Chem.* **2004**, *69*, 8121. (b) Ichihara, K.; Naruta, Y. *Chem. Lett.* **1995**, 631. (c) Carofiglio, T.; Lubian, E.; Menegazzo, I.; Saielli, G.; Varotto, A. *J. Org. Chem.* **2009**, *74*, 9034.

(31) Lazarides, T.; Charalambidis, G.; Vuillamy, A.; Reglier, M.; Klontzas, E.; Froudakis, G.; Kuhri, S.; Guldi, D. M.; Coutsolelos, A. G. *Inorg. Chem.* **2011**, *50*, 8926.
(32) (a) Kim, D.; Osuka, A. *Acc. Chem. Res.* **2004**, *37*, 735. (b) Aratani, N.; Osuka, A.; Kim, Y. H.; Jeong, D. H.; Kim, D. *Angew. Chem., Int. Ed.* **2000**, *39*, 1458. (c) Ahn, T. K.; Yoon, Z. S.; Hwang, I.-W.; Lim, J. K.; Rhee, H.; Joo, T.; Sim, E.; Kim, S. K.; Aratani, N.; Osuka, A.; Kim, D. *J. Phys. Chem. B* **2005**, *109*, 11223.
(33) Cho, H. S.; Song, N. W.; Kim, Y. H.; Jeoung, S. C.; Hahn, S.; Kim, D.; Kim, S. K.; Yoshida, N.; Osuka, A. *J. Phys. Chem. A* **2000**, *104*, 3287.
(34) (a) Lin, C. Y.; Wang, Y. C.; Hsu, S. J.; Lo, C. F.; Diau, E. W.-G. *J. Phys. Chem. C* **2010**, *114*, 687. (b) Lin, C. Y.; Lo, C. F.; Luo, L.; Lu, H. P.; Hung, C. S.; Diau, E. W.-G. *J. Phys. Chem. C* **2009**, *113*, 755. (c) Lo, C. F.; Luo, L.; Diau, E. W.-G.; Chang, I. J.; Lin, C. Y. *Chem. Commun.* **2006**, 1430.
(35) Barea, E. M.; Caballero, R.; Fabregat-Santiago, F.; de La Cruz, P.; Langa, F.; Bisquert, J. *Chem. Phys. Chem.* **2010**, *11*, 245.
(36) Lee, C. W.; Lu, H. P.; Lan, C. M.; Huang, Y. L.; Liang, Y. R.; Yen, W. N.; Liu, Y. C.; Lin, Y. S.; Diau, E. W.-G.; Yeh, C. Y. *Chem.—Eur. J.* **2009**, *15*, 1403.
(37) Imahori, H.; Iijima, H.; Hayashi, H.; Toude, Y.; Umeyama, T.; Matano, Y.; Ito, S. *ChemSusChem.* **2011**, *4*, 797.
(38) Bard, A. J., Faulkner, L. R., Eds. *Electrochemical Methods: Fundamentals and Applications*; John Wiley & Sons, Inc.: New York, 2001; pp 505−509.
(39) (a) Venkataramanan, N. S.; Suvitha, A.; Nejo, H.; Mizuseki, H.; Kawazoe, Y. *Int. J. Quantum Chem.* **2011**, *111*, 2340. (b) Balanay, M. P.; Kim, D. H. *Phys. Chem. Chem. Phys.* **2008**, *10*, 5121. (c) Gordon, K. C.; Lind, S. J.; Gambhir, S.; Officer, D. L. *Phys. Chem. Chem. Phys.* **2009**, *11*, 5598.
(40) (a) Tian, H. N.; Yang, X. C.; Chen, R. K.; Zhang, R.; Hagfeldt, A.; Sunt, L. C. *J. Phys. Chem. C* **2008**, *112*, 11023. (b) Nazeeruddin, M. K.; Humphry-Baker, R.; Liska, P.; Grätzel, M. *J. Phys. Chem. B* **2003**, *107*, 8981.
(41) (a) Hayashi, H.; Hosomizu, K.; Mantano, Y. *J. Phys. Chem. B* **2004**, *108*, 5018. (b) Hayashi, S.; Eu, S.; Imahori, H. *Chem. Commun.* **2007**, 2069.
(42) Chang, Y. C.; Wang, C. L.; Pan, T. Y.; Hong, S. H.; Lan, C. M.; Kuo, H. H.; Lo, C. F.; Hsu, H. Y.; Lin, C. Y.; Diau, E. W.-G. *Chem. Commun.* **2011**, *47*, 8910.
(43) Katoh, R.; Furube, A.; Yoshihara, T.; Hare, K.; Fujihashi, G.; Takano, S.; Murata, S.; Arakawa, H.; Tachiya, M. *J. Phys. Chem. C* **2004**, *108*, 4818.
(44) Liu, Y.; Lin, H.; Dy, J. T.; Tamaki, K.; Nakazaki, J.; Nakayama, D.; Uchida, S.; Kuboa, T.; Segawa, H. *Chem. Commun.* **2011**, *47*, 4010.
(45) Wu, C. H.; Pan, T. Y.; Hong, S. H.; Wang, C. L.; Kuo, H. H.; Chu, Y. Y.; Diau, E. W.-G.; Lin, C. Y. *Chem. Commun.* **2012**, *48*, 4329.
(46) (a) Bisquert, J. *Phys. Chem. Chem. Phys.* **2003**, *5*, 5360. (b) Bisquert, J.; Zaban, A.; Greenshtein, M.; Mora-Sero, I. *J. Am. Chem. Soc.* **2004**, *126*, 13550. (c) Wang, Q.; Moser, J. E.; Grätzel, M. *J. Phys. Chem. B* **2005**, *109*, 14945.
(47) Griffith, M. J.; Sunahara, K.; Wagner, P.; Wagner, K.; Wallace, G. G.; Officer, D. L.; Furube, A.; Katoh, R.; Mori, S.; Mozer, A. J. *Chem. Commun.* **2012**, *48*, 4145.
(48) van de Langemaat, J.; Frank, A. J. *J. Phys. Chem. B* **2000**, *104*, 4292.
(49) Adachi, M.; Sakamoto, M.; Jiu, J. T.; Ogata, Y.; Isoda, S. *J. Phys. Chem. B* **2006**, *110*, 13872.
(50) (a) Nissofolk, J.; Fredin, K.; Hegfeldt, A.; Boschloo, G. *J. Phys. Chem. B* **2006**, *110*, 17715. (b) Wang, Q.; Zhang, Z.; Zakeeruddin, S. M.; Grätzel, M. *J. Phys. Chem. C* **2008**, *112*, 7084.